



Quasi metal organic framework with highly concentrated Cr_2O_3 molecular clusters as the efficient catalyst for dehydrofluorination of 1,1,1,3,3-pentafluoropropane

Bing Liu, Wenfeng Han*, Xiliang Li, Lichun Li, Haodong Tang, Chunshan Lu*, Ying Li, Xiaonian Li

Industrial Institute of Catalysis, Zhejiang University of Technology, Hangzhou, 310032, People's Republic of China

ARTICLE INFO

Keywords:

Metal organic framework
 Cr_2O_3
 Molecular cluster
 Dehydrofluorination
 1,1,1,3,3-pentafluoropropane

ABSTRACT

Metal-organic frameworks (MOFs) are promising platforms for the application of catalysis with hierarchical porous structures and high surface areas. However, the stability is one of the key challenges for the reactions at elevated temperatures. In the present work, we demonstrate the preparation of Quasi MIL-101 structures with high concentration of Cr_2O_3 molecular clusters (21.7 wt%~54.2 wt%) via calcination in N_2 atmosphere at temperatures between 350 °C and 500 °C. Cr_2O_3 clusters show high activity and stability for the dehydrofluorination of 1,1,1,3,3-pentafluoropropane (HFC-245fa) to 1,3,3,3-tetrafluoropropene (HFO-1234ze). Dehydrofluorination of HFC-245fa is an efficient route for the synthesis of HFO-1234ze. With calcination temperature of 450 °C, the reaction rate of Cr_2O_3 molecular clusters is almost 4 times higher than that of commercial Cr_2O_3 and no significant deactivation was observed. Therefore, this study provides a competitive strategy for the preparation of molecular clusters catalysts with high thermal stability.

1. Introduction

Recently, global warming has been one of the major challenges for the whole society. Consequently, it is attracting increasing attention. Hence, the international community is trying to control the consumption of hydrofluorocarbons (HFCs) which usually possess high global warming potential (GWP) based on 100 year time horizon such as 1300 for 1,1,1,2-tetrafluoroethane (HFC-134a) and 820 for 1,1,1,3,3-pentafluoropropane (HFC-245fa) [1,2]. At present, hydrofluoroolefins (HFOs) with short atmospheric life time, zero ozone depletion potential (ODP) and low global warming potential (GWP) are suggested to be excellent substitutes for HFCs [3]. Particularly, ODP of 1,3,3,3-tetrafluoropropene (HFO-1234ze) is zero and its GWP is only 6 with atmospheric life of less than 15 days. In addition, the physical property of HFO-1234ze is very similar with that of HFC-134a. Therefore, HFO-1234ze is considered as an ideal substitute for HFC-134a and a new generation of green refrigerant [4,5].

Dehydrofluorination of 1,1,1,3,3-pentafluoropropane (HFC-245fa) is a promising route for the synthesis of HFO-1234ze among all the routes for the preparation of HFO-1234ze [6,7] which also provides a potential treatment route for HFC-245fa greenhouse gas. For the selective dehydrofluorination of HFC-245fa, catalyst is the key issue. Usually, for reactions involving corrosive HF and HCl gases, such as

dehydrofluorination reactions [8,9], dehydrochlorination reactions [10–13] and chlorine/fluorine exchange reactions [14,15], fluorinated Cr_2O_3 and metal fluorides are adopted [16,17] due to their stability in HCl and HF atmospheres. AlF_3 , MgF_2 and fluorinated Cr_2O_3 [18–21] are the most common catalysts in the fluorine chemical industry. As a strongest solid Lewis acid, although AlF_3 exhibits high activity for the dehydrofluorination and chlorine/fluorine exchange reactions, it also readily promotes the coke formation leading to the deactivation of catalysts [22]. MgF_2 is another potential catalyst with relatively weak Lewis acidity [23]. Unfortunately, MgF_2 sinters significantly at temperatures above 280 °C [24,25] which leads to the rapid deactivation during reactions [26]. To improve the stability, air was added into the reaction system for the removal of coke deposition during dehydrofluorination reactions [27]. However, the addition of air results in the low selectivity and high separation cost. Clearly, the development of proper catalytic materials is of significance for the dehydrofluorination HFCs to HFOs.

More recently, metal-organic frameworks (MOFs) consisted of inorganic nodes and organic linkers [28–30], has attracted increasing attention as the catalytic materials with high surface area, adjustable pore sizes, controllable structures and facile functionalization [31,32]. It is well known that catalytic activity can be improved by increasing the number of exposed active sites [33,34]. Consequently, single-atom

* Corresponding authors.

E-mail addresses: hanwf@zjut.edu.cn (W. Han), lcszjcn@zjut.edu.cn (C. Lu).

<https://doi.org/10.1016/j.apcatb.2019.117939>

Received 7 May 2019; Received in revised form 25 June 2019; Accepted 6 July 2019

Available online 08 July 2019

0926-3373/ © 2019 Elsevier B.V. All rights reserved.

catalysts (SACs) represent the best atomic utilization rate and the lowest size to expose the active sites in catalysts. Preparation of SACs is the emerging topic in the catalysis research [35,36]. MOFs are proper precursors for the preparation of single atom catalysts. As reported by Li [37], isolated single-atom iron catalyst and high oxide reduction reaction (ORR) reactivity were achieved by loading iron to ZIF-8. Jiang [38] prepared an isolated single-atom zinc catalyst and presented excellent performance for carbon dioxide conversion. Ultrahigh loading (11.3 wt%) of single Zn atoms was obtained via the pyrolysis of ZIF-8.

To the best of our knowledge, there is no reports on the gas-phase dehydrofluorination reactions of HFCs over MOFs derived catalysts. In the present study, catalysts derived from Cr-based MOF (MIL-101) [39] for the dehydrofluorination reactions of HFCs were attempted. Molecular Cr_2O_3 clusters encapsulated in the quasi MIL-101 were obtained via the pyrolysis of MIL-101. The effects of morphology, structure, physical and chemical properties of MIL-101-X (X = 350, 400, 450 and 500 °C) on the catalytic dehydrofluorination of HFC-245fa to HFO-1234ze were investigated. Catalysts in the form of Cr_2O_3 molecular clusters confined in the framework of quasi MIL-101 were fabricated following the calcination of MIL-101 at elevated temperatures. Cr_2O_3 clusters with size of less than 1 nm confined in the framework of MIL-101 show high stability under high-temperature reaction conditions. It is worth noting that the Cr_2O_3 molecular clusters prevent the coke formation during the dehydrofluorination of HFC-245fa reaction effectively.

2. Experimental section

2.1. Synthesis of MIL-101

MIL-101 ($\text{Cr}_3\text{F}(\text{H}_2\text{O})_2\text{O}[(\text{O}_2\text{C})\text{C}_6\text{H}_4(\text{CO}_2)]_3 \cdot n\text{H}_2\text{O}$, $n \approx 25$) was prepared according to a previously reported procedure [40]. MIL-101 were synthesized via hydrothermal reaction of $\text{Cr}(\text{NO}_3)_3 \cdot 9\text{H}_2\text{O}$ (8.002 g, 20.0 mmol) with terephthalic acid (3.322 g, 20.0 mmol) in the presence of deionized water (160 mL) and HF (0.9 mL, 40 wt%). The mixed solution was first introduced into a 250 mL Teflon-lined autoclave and heated at 220 °C for 8 h. Then, the solution was cooled to room temperature slowly and the green powder was separated from the solution by centrifugation. The excessive terephthalic acid inside the pores of MIL-101 was removed by the washing with ethanol, DMF and NH_4F (30 mmol L^{-1}) successively. For the washing, firstly the green paste was dispersed in 500 mL DMF at 70 °C for 12 h, followed by cooling. The green powder was separated from DMF by centrifugation. Finally, the washing was repeated with ethanol and NH_4F solution several times (30 mmol L^{-1}) instead of DMF. The green solid was further purified with 1000 mL of deionized water to eliminate traces amounts of NH_4F . Following drying at 80 °C for 12 h under vacuum, the MIL-101 was ready.

2.2. Preparation of quasi MIL-101

MIL-101 underwent pyrolysis in a tube furnace with N_2 atmosphere at 350 °C, 400 °C, 450 °C and 500 °C for 3 h, respectively. During the pyrolysis, MIL-101 was heated from room temperature to desired temperatures with a ramp rate of 3 °C min^{-1} and maintained at desired temperatures for 3 h under flowing N_2 (50 mL min^{-1}), followed by natural cooling to room temperature. Based on the pyrolysis temperatures, the samples were denoted as MIL-101-350, MIL-101-400, MIL-101-450 and MIL-101-500 respectively. The obtained samples were adopted as the catalysts directly without any further treatment. The preparation procedure of quasi MIL-101 samples were schematically illustrated in Scheme 1 and Fig. S1. Following increase in pyrolysis temperature, the color of the sample turned from green to black indicating the gradual carbonization of MIL-101.

2.3. Characterization of catalysts

X-ray diffraction (XRD) analysis was performed with a Thermo ARL X'TRA diffractometer using $\text{Cu-K}\alpha$ radiation ($\lambda = 0.154056 \text{ nm}$) at room temperature, equipped with a Si (Li) solid detector at 40 kV/40 mA with a monochromator. The patterns were taken in a 2θ range from 2° to 80° with the scanning rate of 2° min^{-1} .

Specific surface areas were determined by the modified BET method from N_2 adsorption isotherms at liquid nitrogen temperature (−195.7 °C) on an Autosorb-1/C gas adsorption analyzer (Quantachrome Instruments). Prior to the measurement, the samples were degassed at 200 °C for 5 h under vacuum.

Surface acidity was determined by NH_3 -TPD technique (ammonia temperature-programmed desorption), which was carried out on a fixed-bed reactor (i. d. = 5 mm) containing 50 mg of the catalyst. The sample was heated from 30 to 300 °C at a rate of 10 °C min^{-1} , and kept at 300 °C for 2 h followed by cooling to 100 °C in a flow of Ar (30 mL min^{-1}). NH_3 -He mixture (5% NH_3 , 30 mL min^{-1}) was introduced to the reactor for 2 h to allow the complete adsorption of NH_3 . Prior to measurement, the sample was purged with pure Ar (30 mL min^{-1}) for 60 min to remove physically absorbed NH_3 for 60 min. After cooling down to room temperature, the sample was heated in the Ar flow (30 mL min^{-1}) from 30 to 800 °C with a heating rate of 10 °C min^{-1} , and the desorption of NH_3 was recorded by a mass spectrometer (Omnistar-200) with m/e of 17.

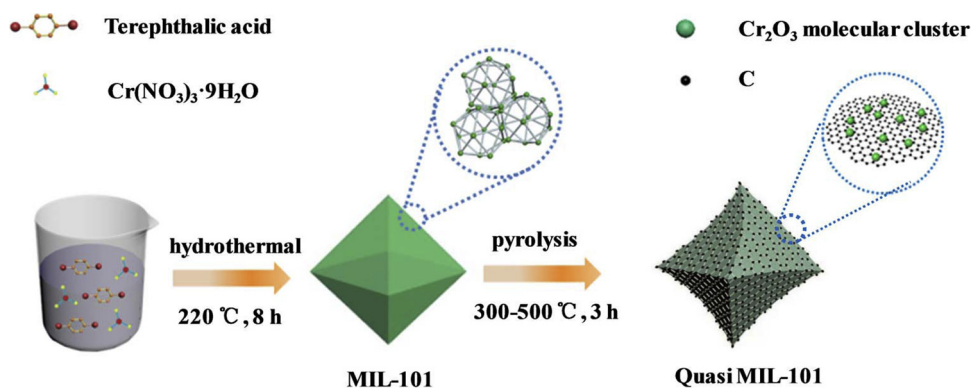
X-ray photoelectron spectroscopy (XPS, ESCALAB210, VG Co., photoelectron spectroscopy with a monochromatized microfocused Mg K α -ray source) was employed to study the binding energy of Cr and C in the catalysts. The binding energy values were adjusted for charging effect by referring to the adventitious carbon (C 1s) at 284.50 eV. Prior to the measurements, the sample pressed into self-supporting disks, was loaded into a subchamber and then evacuated at 25 °C for 6 h.

Thermogravimetric analysis (TG) was measured on a Netzsch STA 409 thermo-analyzer equipped with an online mass spectrometer (MS). Before the experiment, the sample was purged with Ar at 110 °C for 1 h to remove the water of the sample, then switched to the air flow. During the measurement, the samples were heated from 110 °C to 700 °C with a heating rate of 10 °C min^{-1} .

Scanning electron microscopy (SEM) images were obtained on a scanning electron microscope (FESEM, HitachiS-4700) at an accelerating voltage of 15 kV equipped with an X-ray energy spectrometer (EDS). Transmission electron microscopy (TEM) and HRTEM images were recorded by a Tecnai G2 F30 S-Twin of Philips-FEI Company at 300 kV.

2.4. Catalytic activity evaluation

The catalytic experiments was conducted on a fixed bed reactor (stainless steel, 8 mm (i.d)*400 mm) under atmospheric pressure. The temperature uniform zone of the reactor was determined to be 100 mm. A thermal couple was placed in the middle of the catalyst bed to detect the actual reaction temperature. The blank experiments showed that no obvious reactions were found. Prior to the reactions, the catalysts were first activated. 1 mL of the catalyst (20–40 mesh) was loaded into the reactor and heated at 300 °C for 1 h in N_2 with a flow rate of 10 mL min^{-1} . Then the catalyst was activated with chlorodifluoromethane (HCFC-22) balanced by N_2 at 300 °C for 2 h ($\text{HCFC-22}/\text{N}_2$ of 1 with total flow rate of 20 mL min^{-1}). Following activation of the catalysts, the reaction temperature was increased to 350 °C. A mixed HFC-245fa/ N_2 gas was fed into the reactor (HFC-245fa/ N_2 of 4/10, total flow rate of 12.5 mL min^{-1} , SV = 750 h^{-1}). The products formed during the reaction were passed through a KOH solution to trap HF, and then the gaseous products were analyzed by an online gas chromatograph (Fuli GC9790) equipped with a PoraPLOT Q column and a TCD (thermal conductivity detector).



Scheme 1. Schematic illustration of the preparation of quasi MIL-101.

3. Results and discussion

The metal-organic framework MIL-101 (Cr) was successfully prepared via hydrothermal reaction of $\text{Cr}(\text{NO}_3)_3 \cdot 9\text{H}_2\text{O}$ with terephthalic acid in the presence of HF and deionized water. Following hydrothermal reaction, smooth and clean octahedral crystals (the typical morphology of MIL-101) were obtained (Figs. 1a and S2a and b). The

diameter of the octahedral morphology crystals ranges from 380 nm to $1.5\text{ }\mu\text{m}$, with average diameter of about 694 nm (Fig. S3). Following calcination at temperatures of $350\text{ }^\circ\text{C}$, $400\text{ }^\circ\text{C}$, $450\text{ }^\circ\text{C}$ and $500\text{ }^\circ\text{C}$ in N_2 atmosphere for 3 h, the octahedral crystals collapse significantly with different extents. Clearly, the collapse extent increases with calcination temperature. Although octahedral structures are identifiable, clear shrinkage is noted (Fig. 1b–d and Fig. S2c–j). During calcination, partial

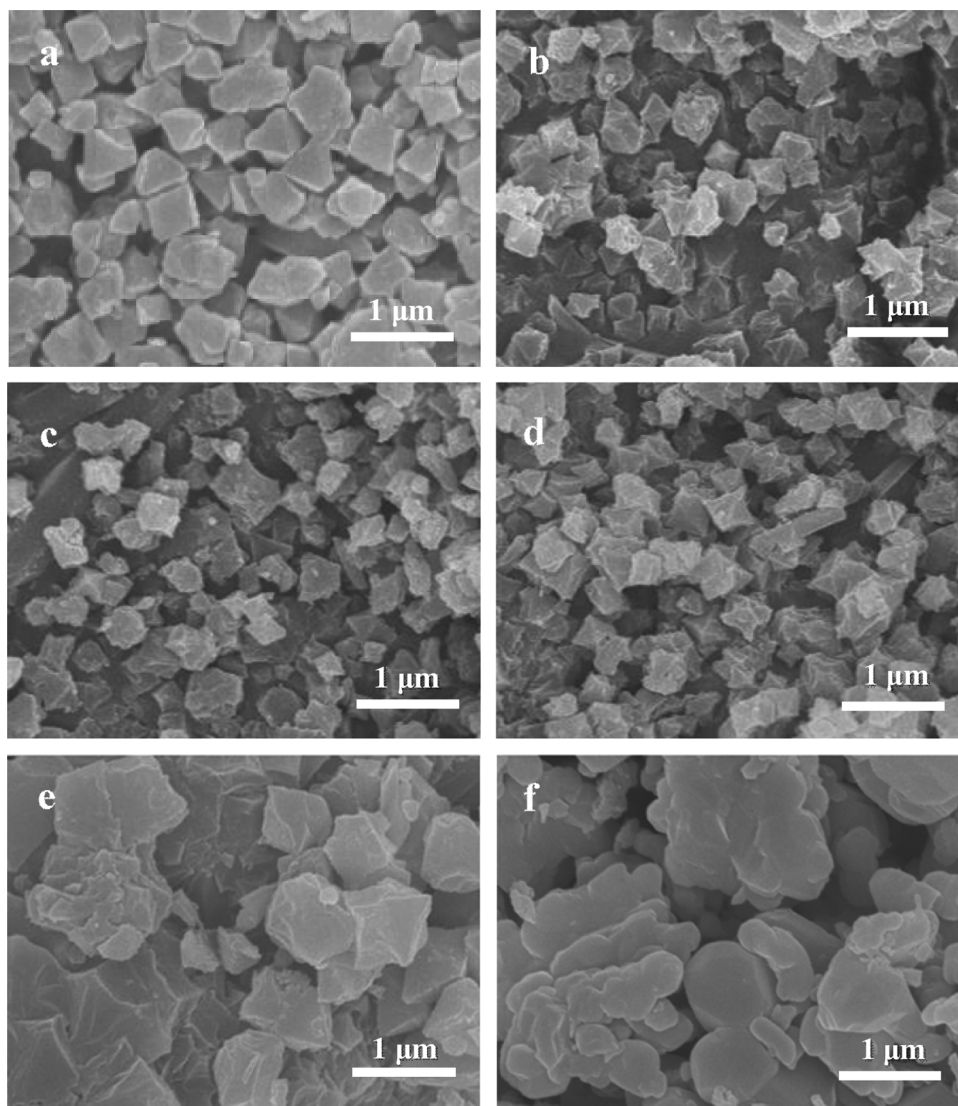


Fig. 1. SEM images of (a) MIL-101, (b) MIL-101-350, (c) MIL-101-400, (d) MIL-101-450, (e) MIL-101-500 and (f) Commercial Cr_2O_3 .

Table 1

Elemental composition of the MIL-101, quasi MIL-101 and commercial Cr₂O₃ determined by EDS.

Catalyst	Elemental composition, at%			O/Cr
	C	O	Cr	
MIL-101	74.64	21.68	3.68	5.9
MIL-101-350	68.68	27.60	3.72	7.4
MIL-101-400	64.97	26.86	8.17	3.3
MIL-101-450	64.79	23.22	11.99	1.9
MIL-101-500	58.60	27.55	13.85	2.0
Commercial Cr ₂ O ₃	—	59.81	40.19	1.5

deligandation of MIL-101 occurred leading to the formation of quasi MIL-101. However, the porous structures and interaction between Cr-O nodes and ligand are still retained [41]. It enables the formation of highly concentrated Cr₂O₃ molecular clusters in quasi MIL-101 structures. Complete collapse is observed with MIL-101(Cr) heated at 500 °C for 3 h (Fig. 1e). As displayed in Fig. 1f, the commercial Cr₂O₃ exhibits irregular particle morphology.

According to the elemental content analysis (EDS), the content of Cr in quasi MIL-101 increase with calcination temperature monotonically (Table 1). It is ascribed to the gradual removal of organic ligands. With the increase in calcination temperature, larger amounts of organic ligands are decomposed and consequently larger amounts of Cr-O nodes are produced. Following calcination at different temperatures, Cr content increases from 3.68% (for MIL-101 without calcination) to 13.85% (for MIL-101-500). However, the Cr concentration of MIL-101-500 is still far lower than that of commercial Cr₂O₃ (40.19%), indicating that significant amounts of ligands or carbonaceous species are remained even with calcination of 500 °C. As listed in Table 1, the content of carbon decreases with calcination temperature (from 74.64% to 58.60%) which reinforces the removal of organic ligands. Similarly, the ratio of O/Cr drops from 5.9 to 2.0 approaching to the value of commercial Cr₂O₃. As part of oxygen-containing ligands are retained in quasi MIL-101, the O/Cr is higher than that of commercial Cr₂O₃.

To further investigate the morphology and the surface properties of the MIL-101(Cr) after calcination at different temperatures (350 °C, 400 °C, 450 °C and 500 °C) in N₂, TEM technique was employed and the results are presented in Fig. 2. Fig. 2a indicates that the as prepared MIL-101(Cr) possesses clean octahedral morphology which agrees well with the morphology in literature [42]. Following calcination at 350 °C, MIL-101-350 retains its initial octahedral shape, while the surface is much rougher reinforcing the partial deligandation of MIL-101 during calcination (Fig. 2b). With the increase of calcination temperature, the deligandation degree of octahedral morphology becomes more and more obvious (Fig. 2c and d). With the calcination at 500 °C (Fig. 2e), the morphology of MIL-101(Cr) collapses completely and sheet-like structures are derived which is consistent with the observation of SEM (Fig. 1). Clearly, commercial Cr₂O₃ exhibits irregular, thick and solid particles which are totally different from quasi MIL-101 obtained by calcination of MIL-101(Cr) at different temperatures (Fig. 2f).

The effect of calcination was further confirmed by TG-DTG experiment. As demonstrated in Fig. 3, the weight loss during calcination of MIL-101(Cr) is divided into three stages. The weight loss at around 200 °C corresponds to the removal of binding water in the sample, which accounts for about 3.43 wt% of the total sample. Following the dehydration, the significant weight loss is observed at temperatures between 340 °C and 440 °C. Clearly, it is attributed to the deligandation of MIL-101 with the weight loss of about 29.3%. Reasonably, this process is responsible for the partial collapse of MIL-101 structure as indicated in the SEM (Fig. 1) and TEM (Fig. 2) images. At around 500 °C, another peak with weight loss of about 1.9 wt% is identified which corresponds to the total carbonization of ligand. With complete decomposition of MIL-101, sheet-like structures are derived (Figs. 1e

and 2 e).

Fig. 4 displays the HRTEM images of calcined MIL-101 at temperatures between 350 °C and 500 °C. Part of the Cr₂O₃ particles are highlighted by yellow circles in the figures. With the calcination temperatures of 350 °C and 400 °C (Fig. 4a and b), densely distributed Cr₂O₃ particles are identified with diameters of 0.47 nm and 0.55 nm respectively (Fig. S5a and b). As the diameter of Cr atom is around 0.2 nm, Cr₂O₃ is almost molecularly dispersed in MIL-101-350 and MIL-101-400. With the calcination temperature of 450 °C (Fig. 4c), the particle size of Cr₂O₃ slightly increases to 0.6 nm (Fig. S5c). Clearly, Cr₂O₃ is in the form of molecular cluster. It is reinforced by the elemental mapping analysis (EDX) that C, O and Cr are uniformly distributed (Fig. S4). Following the calcination of 500 °C, Cr₂O₃ takes place significantly sintering. As demonstrated in Figs. 4d and S5d, the particle size is around 1.67 nm for MIL-101-500. This result was supported by the results of XRD and SEM.

The Cr₂O₃ molecular clusters rather than crystals are further confirmed by selected area electron diffraction (SEAD). As indicated in Fig. S6f and i, SEAD patterns of MIL-101-350 and MIL-101-400 exhibit halo-like images, implying the amorphous structures of the corresponding samples. Clearly, Cr₂O₃ molecule clusters are too small to form crystals. In addition, it is consistent with the results of XRD. As illustrated in Fig. 5a, following calcination between 350 °C and 500 °C, no characteristic peaks of Cr₂O₃ and other impurities are detected by the XRD patterns, indicating the high degree of Cr³⁺ disorder and amorphous phase of MIL-101(Cr) after calcination. It is worth noting the ultrahigh loading of chromium at the MIL-101-X. As listed in Table 1, the content is as high as 3.7 at% and 13.9 at%, corresponding to the loading of 21.7 wt% to 54.2 wt%. Such high loading is difficult to be achieved by conventional impregnation while maintaining molecular structure or sub-nanoscale.

The XRD pattern of MIL-101 prepared in this study agrees well the reported results [40,43]. Following calcination at 350 °C, broadening of the diffraction peaks around 5–10° for MIL-101 was observed, implying the incipient deligandation of MIL-101 which is consistent with the observation of SEM (Figs. 1 and S2). However, according to the XRD pattern of MIL-101-350, basic MIL-101 is still retained after calcination at 350 °C. With the calcination temperature increasing to 400 °C, only one weak and broad diffraction peak is identified for MIL-101-400, indicating the significant deligandation of the MIL-101 framework. Following calcination at 450 °C, the characteristic peaks of MIL-101 disappear completely. Clearly, MIL-101 framework collapses significantly. However, even with the calcination temperature of 500 °C, no characteristic peaks of Cr₂O₃ are detected (MIL-101-500). Consistent with TEM observation in Figs. 4 and S6, the particle sizes of Cr₂O₃ molecular clusters are too small to be detected by XRD. By contrast, commercial Cr₂O₃ is in the form of irregular and solid particles, and strong diffraction peaks are observed which agree well with that of Cr₂O₃ (Fig. 5b).

The specific surface area and pore structure of MIL-101, quasi MIL-101 with calcination at different temperatures as well as the commercial Cr₂O₃ were investigated by N₂ physisorption experiments. As shown in Fig. 6a, the MIL-101 exhibits type I isotherms according to the IUPAC classification, which is indicative of the presence of micro pores with the pore diameter between 1 to 2 nm (Fig. S7a) and the specific surface area of MIL-101 is estimated to be about 2965 m²/g (Table S1). Clearly, the N₂ adsorption-desorption isotherms Figs. 6b and S7b further confirm the partial collapse of MIL-101 following calcination between 350 °C and 500 °C. As displayed in Fig. 6b, the N₂ adsorption decreases with calcination temperature which is well consistent with the results of SEM and TEM in Figs. 1 and 2. In addition, the specific surface area also drops significantly upon calcination (Table S1). With calcination at 350 °C, the specific surface area of MIL-101-350 decreases from 2965 m²/g to 415 m²/g. With further increase in the calcination temperature to 500 °C, the specific area of MIL-101-500 further declines to 236.6 m²/g. Clearly, although the Cr₂O₃ molecular clusters

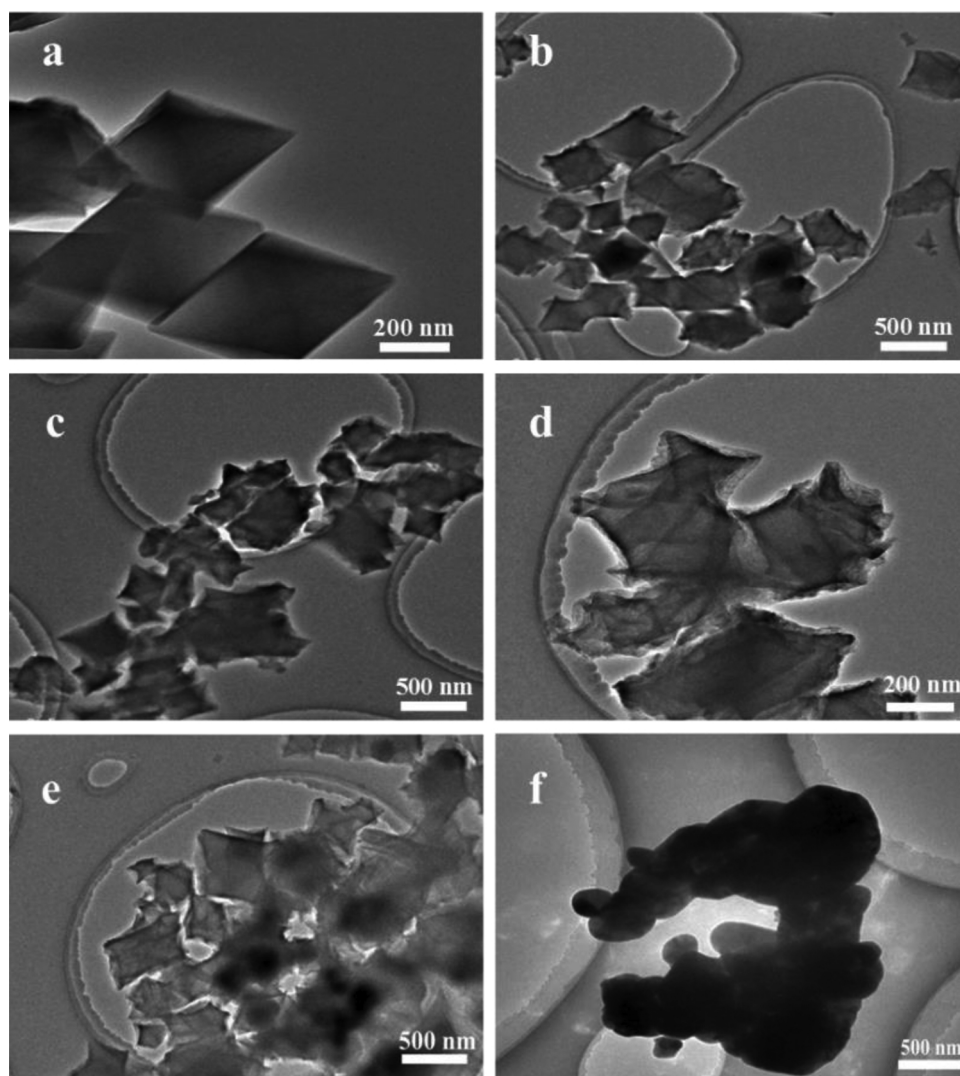


Fig. 2. TEM images of (a) MIL-101, (b) MIL-101-350, (c) MIL-101-400, (d) MIL-101-450, (e) MIL-101-500 and (f) commercial Cr_2O_3 .

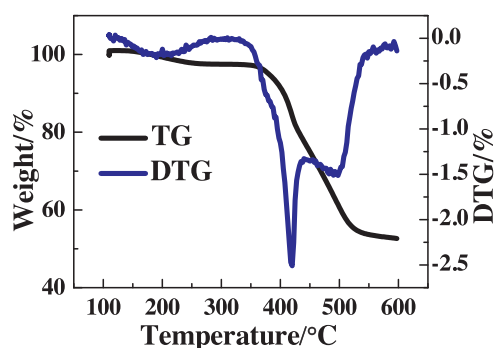


Fig. 3. TG-DTG of MIL-101(Cr) with ramp rate of $10^\circ\text{C}/\text{min}$ in N_2 atmosphere.

are confined in the quasi MIL-101 structures, the relatively high surface and developed pore structure of quasi MIL-101 structures facilitate the exposure of the Cr_2O_3 molecular clusters. As listed in Table S1, commercial Cr_2O_3 exhibits rather low surface area ($2.3 \text{ m}^2/\text{g}$).

MIL-101, MIL-101-450 and commercial Cr_2O_3 catalysts were further characterized by XPS for the investigation of surface chemistry. The surface elemental contents determined by XPS were listed Table S2 which agree well the results of EDS in Table 1. Fig. 7 demonstrates the Cr 2p XPS spectra for these catalysts. For MIL-101, as displayed in

Fig. 7a, only one Cr $2p_{3/2}$ peak is detected. Consequently, there is only one Cr species in MIL-101. The peak with binding energy around 576.5 eV is assigned to $[\text{Cr}(\text{CO})_x]$ species [41,44] which well corresponds to $[\text{Cr}_3\text{O}(\text{CO}_2)_6]$, the basic unit of MIL-101 [39]. For MIL-101-450, Cr $2p_{3/2}$ peak is deconvoluted into three peaks with binding energies at about 576.3 eV, 577.4 eV and 578.6 eV respectively, attributing to the $[\text{Cr}(\text{CO})_x]$, Cr_2O_3 [45] and CrO_3 [46,47] respectively (Fig. 7b). Clearly, according to the spectrum, significant amounts of $[\text{Cr}_3\text{O}(\text{CO}_2)_6]$ structures decompose into Cr_2O_3 and CrO_3 . However, large amounts of pristine structures are retained at 450 $^\circ\text{C}$. The binding energy of $[\text{Cr}(\text{CO})_x]$ shifted from 576.5 eV to 576.3 eV following calcination. It can be ascribed to the calcination of the MIL-101(Cr). After calcination, the coordination environments of Cr by deligandation of MIL-101 were changed. More organic ligands of the MIL-101 were removed and the framework of MIL-101 was collapsed. As a result, the interaction of the Cr with MIL-101 framework becomes more weaker and the peak position of the $[\text{Cr}(\text{CO})_x]$ shifts to lower energy. In addition, XPS spectrum of MIL-101-450 clearly confirms the formation of Cr_2O_3 which reinforces that the fine dots in HRTEM images corresponds to the clusters of Cr_2O_3 . As shown in Fig. 7c, the commercial Cr_2O_3 exhibits three peaks at binding energies about 575.9 eV, 577.18 eV and 578.56 eV, indicating the existence of $\text{Cr}(\text{OH})_3$ [48,49], Cr_2O_3 , and CrO_3 respectively. It is noted that the binding energy of Cr_2O_3 in MIL-101-450 is slightly higher than that of the commercial Cr_2O_3 . This

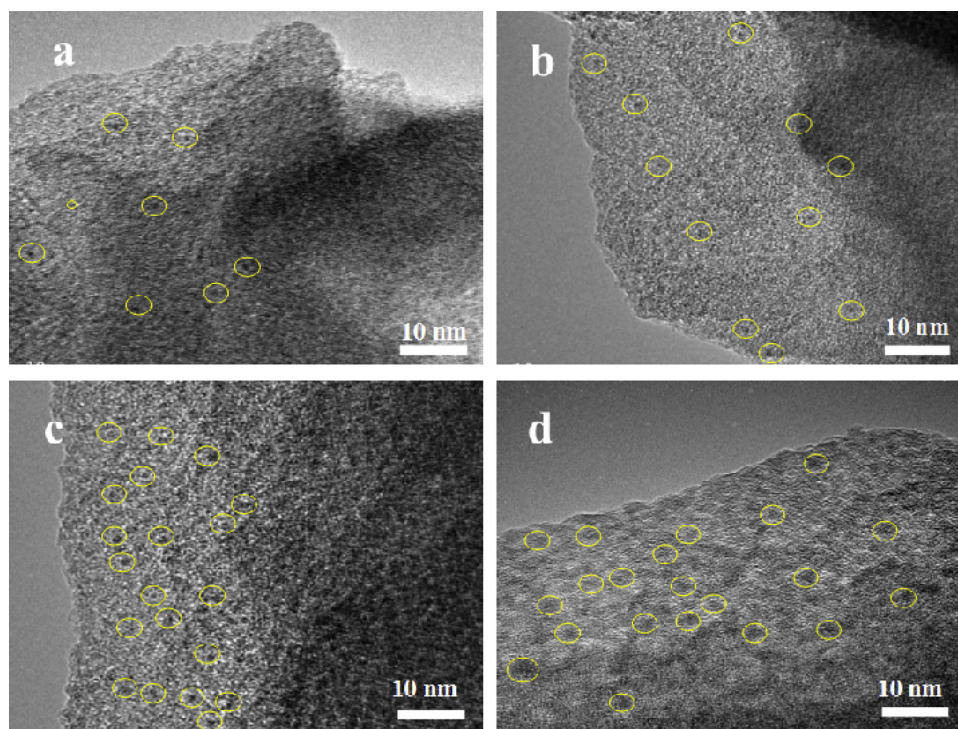


Fig. 4. HRTEM images of (a) MIL-101-350, (b) MIL-101-400, (c) MIL-101-450 and (d) MIL-101-500.

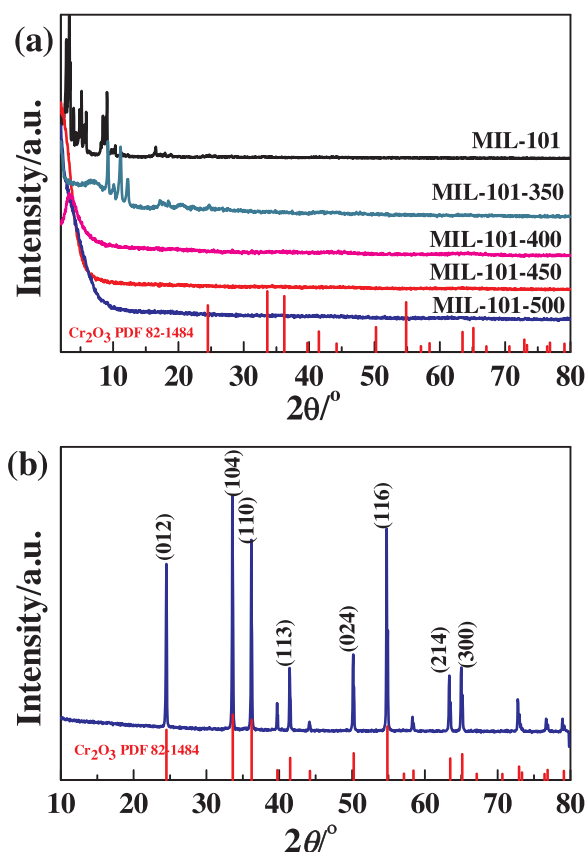


Fig. 5. XRD patterns of (a) MIL-101 and MIL-101-X (b) commercial Cr_2O_3 .

difference is attributed to the interaction between Cr_2O_3 and quasi MIL-101 framework. This result also confirms that the Cr_2O_3 molecular clusters are confined in the framework of quasi MIL-101 which renders high thermal stability to the Cr_2O_3 molecular clusters.

Unexpectedly, quasi MIL-101 structures show high activity and stability for the dehydrofluorination of 1,1,1,3,3-pentafluoropropane (HFC-245fa) to 1,3,3,3-tetrafluoropropene (Figs. S8 and S9a). All the catalysts show similar selectivity (Fig. S9b). The catalytic activities over quasi MIL-101 and commercial Cr_2O_3 catalysts were evaluated at temperature 350°C , atmospheric pressure and gas hourly space velocity (GHSV) of 750 h^{-1} . The reaction rates as a function of time on stream (TOS) are illustrated in Fig. 8a. Although commercial Cr_2O_3 exhibits relatively high activity initially, it decreases with time on stream monotonically. Within TOS of 20 h, the reaction rate drops from $3\text{ mmol h}^{-1}\text{ g}^{-1}$ to less than $1\text{ mmol h}^{-1}\text{ g}^{-1}$. By contrast, quasi MIL-101 shows stable activity excluding MIL-101-500. As argued previously, although the initial activity is high, the MIL-101 structure is totally collapsed, resulting in sintered Cr_2O_3 particles. Consequently, relatively poor stability is obtained for MIL-101-500. For other quasi MIL-101 structures, the activity increases with calcination temperature (Fig. S9c). With calcination temperature of 450°C , the reaction rate of about $4.5\text{ mmol h}^{-1}\text{ g}^{-1}$ is achieved which is almost 4 times higher than that of commercial Cr_2O_3 . Clearly, with elevated calcination temperature, more ligands are carbonized which renders the enhanced exposure of Cr sites. Hence, high activity is approached. However, with calcination at 500°C , full decomposition of MIL-101 is resulted which causes the significant sintering of Cr_2O_3 . In addition, MIL-101-450 presents stable selectivity with the selectivity to trans-HFO-1234ze of c.a. 78% and to cis-HFO-1234ze of c.a. 22% (Fig. 8b). The performance of MIL-101-450 is highly competitive compared with literature (Table S3). Although Cr_2O_3 molecular clusters are all achieved, quasi MIL-101 structures are not well developed at calcination temperatures of 350°C and 400°C , and therefore MIL-101-350 and MIL-101-400 exhibit relatively low activity compared with that of MIL-101-450 (Fig. S9a and d). It is worth noting that reaction temperature also plays an important role. The conversion of HFC-245fa increases with greatly and conversion levels of higher than 80% are approached at reaction temperatures above 425°C (Fig. 8c).

It is widely accepted that the dehydrogenation reactions of hydrofluorocarbons are catalyzed by the Lewis acidic sites [50]. The catalytic activity of carbon itself is excluded (Fig. S10). Therefore, the acidity of

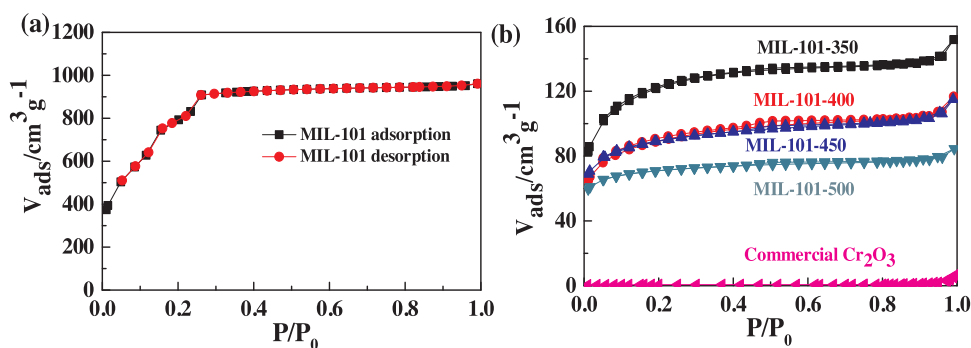


Fig. 6. (a) N_2 adsorption-desorption isotherms of MIL-101(Cr), (b) N_2 adsorption-desorption isotherms of quasi MIL-101 and Commercial Cr_2O_3 .

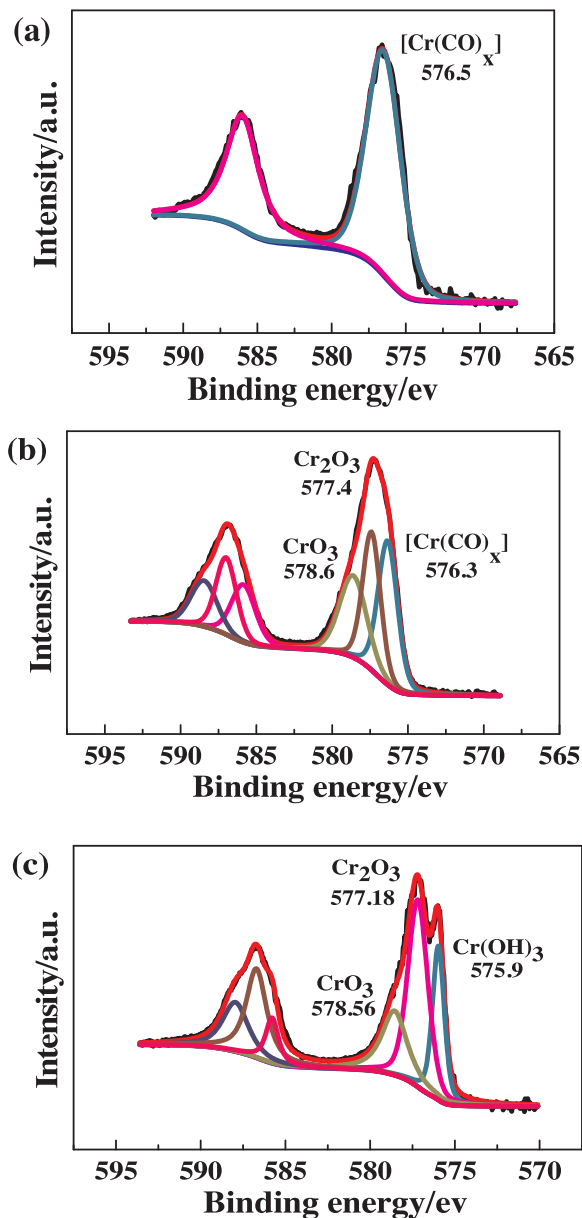


Fig. 7. Cr 2p XPS spectra of (a) MIL-101, (b) MIL-101-450 and (c) commercial Cr_2O_3 .

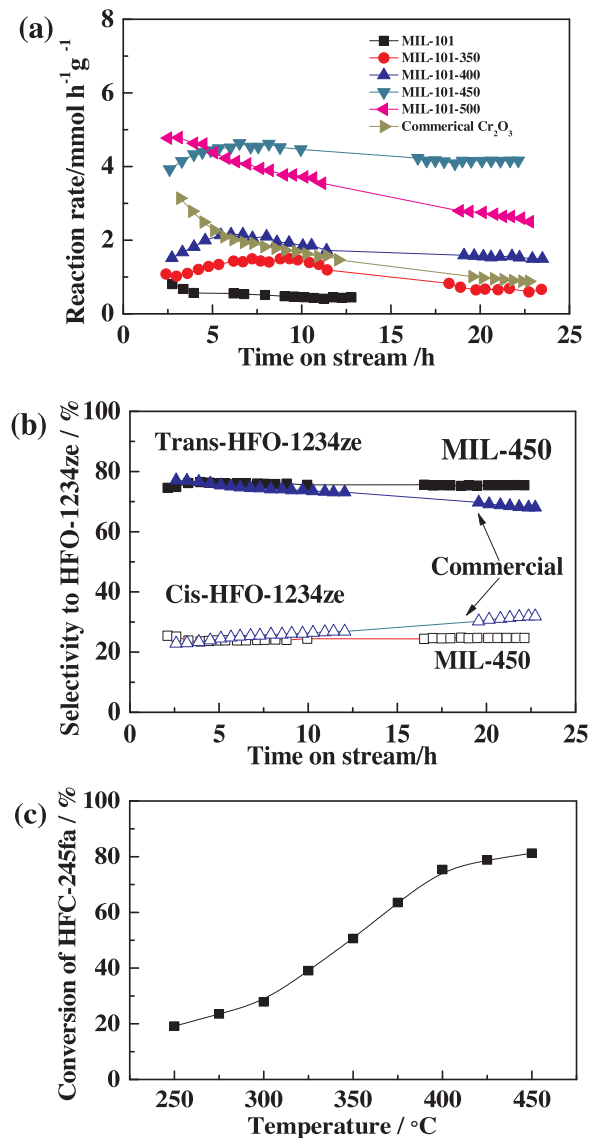


Fig. 8. (a) Reaction rate of HFC-245fa dehydrofluorination over MIL-101 and quasi MIL-101 and commercial Cr_2O_3 as a function of time on stream (atmospheric pressure, 750 h^{-1} with the feed gas composition of 20% HFC-245fa and 80% N_2). (b) Selectivities of HFO-1234ze (E) and HFO-1234ze (Z) over MIL-101-450 and commercial Cr_2O_3 as a function of time on stream. (c) Conversion of HFC-245fa over MIL-101-450 as a function of temperature (atmospheric pressure, 750 h^{-1} with the feed gas composition of 20% HFC-245fa and 80% N_2).

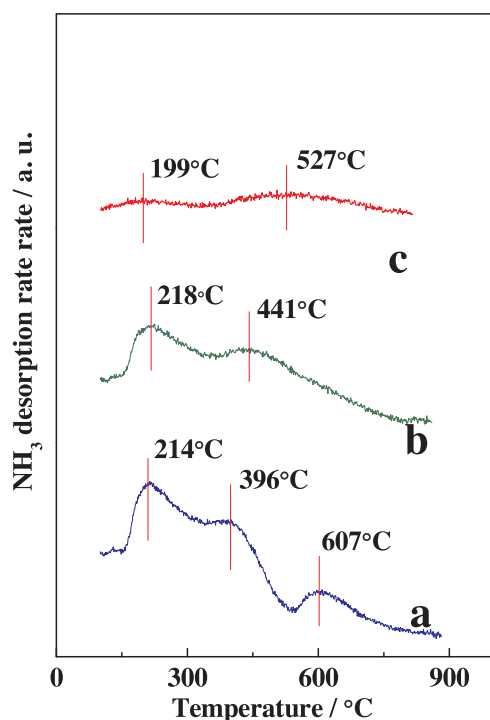


Fig. 9. NH_3 -TPD profiles of (a) MIL-101-350, (b) MIL-101-450 and (c) MIL-101-500.

MIL-100-350, MIL-101-450 and MIL-101-500 was characterized by the NH_3 -TPD technique (Fig. 9). The NH_3 -TPD profiles reveal that the MIL-101-450 catalyst shows two broad desorption peaks at temperature range of 200–450 °C, which suggests that the catalyst contain mild acidic sites. For MIL-100-350, three NH_3 desorption peaks were detected with peak temperatures at 241 °C, 396 °C and 607 °C, respectively, corresponding to the weak and strong acid sites. As noted previously, strong acid sites are responsible for the formation of coke and polymer-like deposition. Hence, the catalytic activity and stability of catalyst of the MIL-100-450 were higher than that of MIL-100-350. And the NH_3 desorption peak at 241 °C of MIL-100-350 is sharper than the corresponding NH_3 desorption peak at 218 °C of MIL-100-450. It indicates that the diameter of the Cr_2O_3 clusters of MIL-101-350 is smaller than MIL-101-450. However, the two ammonia desorption peaks of the MIL-100-500 at 199 and 527 °C are weaker, indicating that there were small amounts of acidic sites on the surface of MIL-100-500.

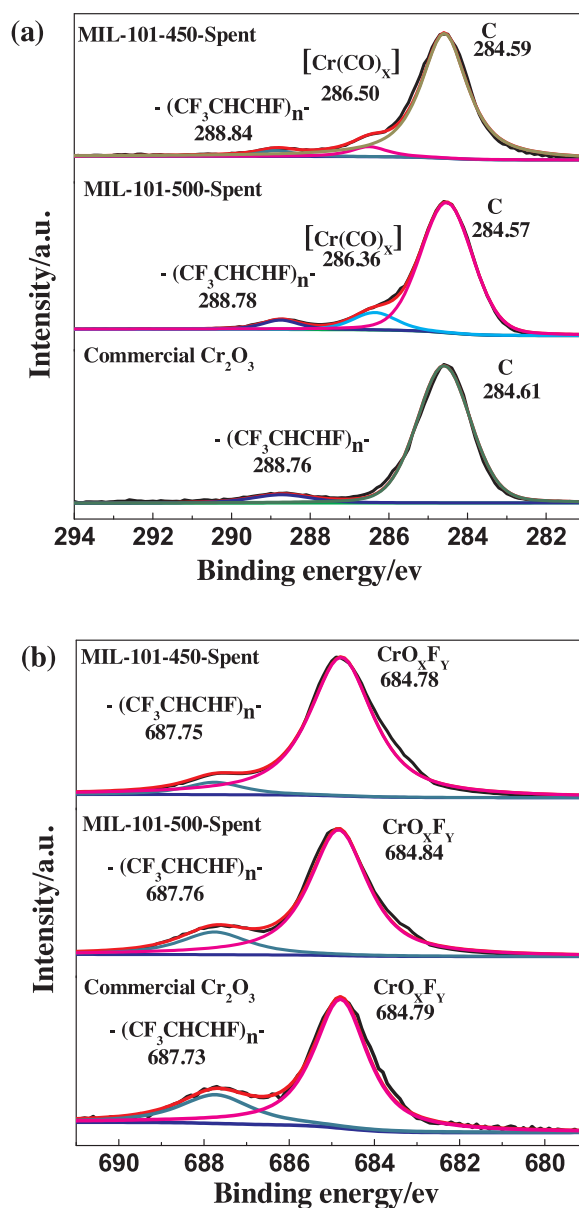
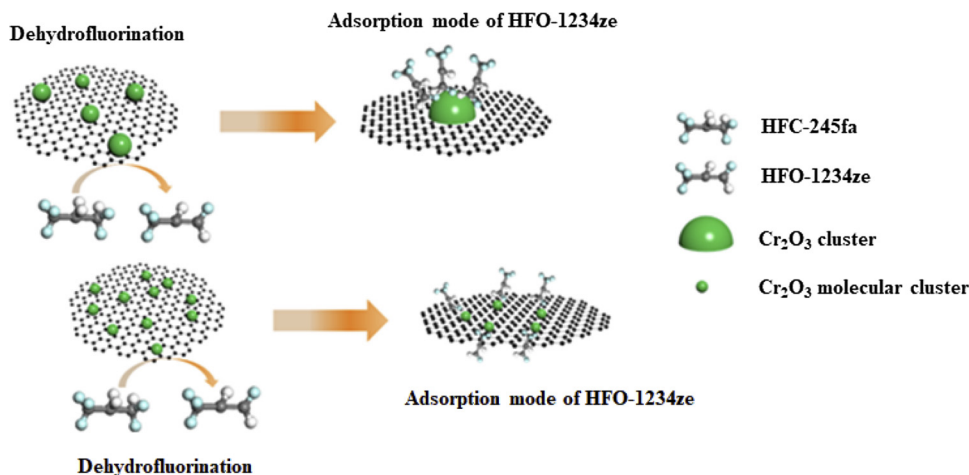


Fig. 10. XPS spectra of spent quasi MIL-101 and commercial Cr_2O_3 , (a) C 1s and (b) F 1s.



Scheme 2. Schematic illustration of the coke formation mechanism of MIL-101-X (X = 350, 400, 450 and 500 °C) catalysts for HFC-245fa dehydrofluorination to HFO-1234ze.

Table 2
Surface element content of spent quasi MIL-101 and commercial Cr₂O₃ determined by XPS.

Catalysts	C species/mol%			F species/mol%	
	-[CF ₃ CHCHF] _n	[Cr(CO) _x] _n	C	-[CF ₃ CHCHF] _n	CrO _x F _y
MIL-101-450	3.2	5.77	91.03	7.52	92.48
MIL-101-500	5.1	10.1	84.8	17.68	82.32
Commercial Cr ₂ O ₃	8.2	0	91.8	24.3	75.7

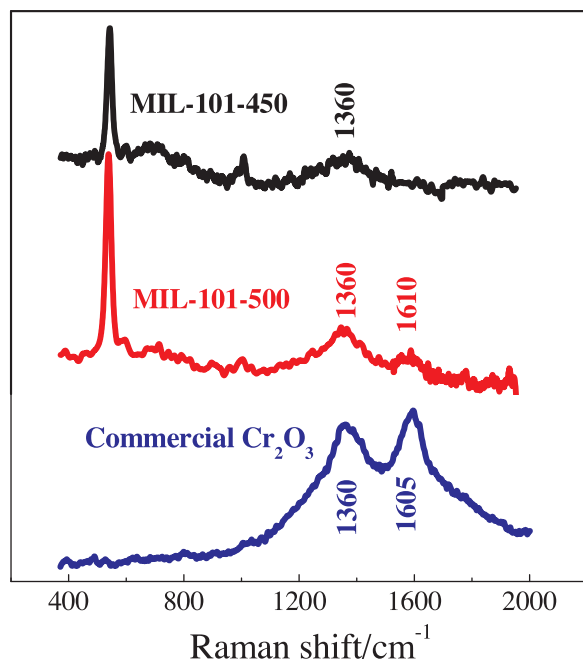


Fig. 11. Raman spectra of spent quasi MIL-101 and commercial Cr₂O₃.

This can be ascribed to sintering because of the increased calcination temperature. In the absence of strong acidic sites over MIL-100-500, high stability is expected. In addition to the acidic sites, we suggested that the particle size of Cr₂O₃ play a major role in the deactivation.

We suggest that small Cr₂O₃ sizes inhibits the formation of coke. For the olefin involving reactions, the formation of polymer like structures is responsible for the coke deposition [51]. As illustrated in Scheme 2, following dehydrofluorination reaction, HFO-1234ze molecules with double bonds are adsorbed over the active sites. With large catalyst particles, multiple and adjacent sites are available with the adsorption of products. Under reaction conditions, the polymerization and desorption of products compete with each other. As a result, the surface of the catalyst is covered by layers of polymer-like deposition. By contrast, with Cr₂O₃ molecular clusters as the catalyst, the active sites are isolated by quasi MIL-101 structure, and the adjacent sites are relatively rare. Consequently, the coupling of olefin products and formation of polymer-structures are inhibited. Hence, Cr₂O₃ molecular clusters exhibit high activity and stability.

To verify the above discussion, the spent MIL-101-450, MIL-101-500 and commercial Cr₂O₃ catalysts were further characterized by XPS and Raman for the investigation of surface chemistry. Fig. 10a demonstrates the C 1s XPS spectra for these catalysts. For spent MIL-101-450, MIL-101-500 and commercial Cr₂O₃ catalysts, C 1s peaks were deconvoluted into three peaks with binding energies at about 284.59–284.57 eV, 286.5–286.36 eV and 288.84–288.78 eV respectively, attributing to the C [52], [Cr(CO)_x]_n and -(CF₃CHCHF)_n-. Clearly, as listed in Table 2, carbon deposition over MIL-101-500 and commercial Cr₂O₃ is significantly higher than that of MIL-101-450. Especially, carbon

depositions derived from polymerization over MIL-101-500 and commercial Cr₂O₃ are 57% and 69% higher than MIL-101-450 respectively (based on the -[CF₃CHCHF]_n- in F 1s spectra (Fig. 10b)).

This argument is reinforced by Raman spectra. As displayed in Fig. 11, polymerization of olefin by C=C double bonds (the peaks with Raman shift of 1610 cm⁻¹ and 1605 cm⁻¹) is identified over spent MIL-101-500 and commercial Cr₂O₃ [53], while no obvious peak is observed at 1610 cm⁻¹ for spent MIL-101-450. Clearly, it indicates that Cr₂O₃ molecular clusters in MIL-101-450 inhibits the polymerization and coke formation.

4. Conclusions

MIL-101 structure was synthesized by hydrothermal method with Cr(NO₃)₃·9H₂O as the precursors and terephthalic acid as the organic ligands. Quasi MIL-101 structures (MIL-101-350, MIL-101-400, MIL-101-450 and MIL-101-500) were obtained by calcination in N₂ atmosphere and temperatures between 350 °C and 500 °C. Following calcination, Cr₂O₃ molecular clusters were uniformly distributed and confined over the surface of quasi MIL-101 structures with ultrahigh loading of chromium (21.7 wt%~54.2 wt%). The diameter of Cr₂O₃ clusters less than 1 nm with amorphous structures were obtained. In addition, as Cr₂O₃ clusters were confined in the framework of quasi MIL-101, Cr₂O₃ clusters show high activity and stability for the dehydrofluorination of 1,1,1,3,3-pentafluoropropane (HFC-245fa) to 1,3,3,3-tetrafluoropropene (HFO-1234ze). Although commercial Cr₂O₃ exhibits relatively high activity initially, it decreases with time on stream monotonically. With calcination temperature of 450 °C, the reaction rate of MIL-101-450 is almost 4 times higher than that of commercial Cr₂O₃ and no significant deactivation was observed. This study provides a competitive strategy for the preparation of molecular clusters catalysts with high thermal stability.

Conflict of interest

Nothing declared.

Acknowledgements

This research was supported by Zhejiang Provincial Natural Science Foundation of China under Grant No. LY19B060009.

Appendix A. Supplementary data

Supplementary material related to this article can be found, in the online version, at doi:<https://doi.org/10.1016/j.apcatb.2019.117939>.

References

- [1] G.J.M. Velders, D.W. Fahey, J.S. Daniel, M. McFarland, S.O. Andersen, PNAS 106 (2009) 10949–10954.
- [2] G.J.M. Velders, A.R. Ravishankara, M.K. Miller, M.J. Molina, J. Alcamo, J.S. Daniel, D.W. Fahey, S.A. Montzka, S. Reimann, Science 335 (2012) 922–923.
- [3] M.K. Vollmer, S. Reimann, M. Hill, D. Brunner, Environ. Sci. Technol. 49 (2015) 2703–2708.
- [4] D.J. Lueken, R.L. Waterland, S. Papasavva, K.N. Taddonio, W.T. Hutzell, J.P. Rugh, S.O. Andersen, Environ. Sci. Technol. 44 (2010) 343–348.
- [5] A. Mota-Babiloni, J. Navarro-Esbri, F. Moles, A. Barragan Cervera, B. Peris, G. Verdu, Appl. Therm. Eng. 95 (2016) 211–222.
- [6] Y.X. Cheng, J.L. Fan, Z.Y. Xie, J.Q. Lu, M.F. Luo, J. Fluorine Chem. 156 (2013) 66–72.
- [7] J.-W. Luo, J.-D. Song, W.-Z. Jia, Z.-Y. Pu, J.-Q. Lu, M.-F. Luo, Appl. Surf. Sci. 433 (2018) 904–913.
- [8] W.Z. Jia, Y.F. Chen, M. Liu, X.H. Liu, J.J. Yuan, X.J. Lu, Z.R. Zhu, Appl. Catal. A Gen. 571 (2019) 150–157.
- [9] W. Mao, Y.B. Bai, Z.H. Jia, Z.Q. Yang, Z.J. Hao, J. Lu, Appl. Catal. A Gen. 564 (2018) 147–156.
- [10] Z.K. Wang, W.F. Han, H.D. Tang, Y. Li, H.Z. Liu, Microporous Mesoporous Mater. 275 (2019) 200–206.
- [11] Z.K. Wang, W.F. Han, H.D. Tang, H.Z. Liu, Catal. Commun. 120 (2019) 42–45.
- [12] Z.K. Wang, W.F. Han, C.P. Zhang, S.L. Zhou, H.L. Wang, H.D. Tang, H.Z. Liu,

- Chemistryselect 3 (2018) 1015–1018.
- [13] T.Y. Song, Z.X. Dong, J.D. Song, X.X. Wang, G.Q. Xie, M.F. Luo, J.Q. Lu, Appl. Catal. B 236 (2018) 368–376.
 - [14] W.F. Han, J.C. Wang, L.L. Chen, L.T. Yang, S.C. Wang, M. Xi, H.D. Tang, W.C. Liu, W.Y. Song, J.J. Zhang, Y. Li, H.Z. Liu, Chem. Eng. J. 355 (2019) 594–601.
 - [15] W.F. Han, S.L. Zhou, M. Xi, H.L. Wang, W.C. Liu, H.D. Tang, Z.K. Wang, C.P. Zhang, J. Fluorine Chem. 202 (2017) 65–70.
 - [16] Z.H. Jia, W. Mao, Y.B. Bai, B. Wang, H. Ma, C. Li, J. Lu, Appl. Catal. B 238 (2018) 599–608.
 - [17] J.D. Song, T.Y. Song, T.T. Zhang, Y. Wang, M.F. Luo, J.Q. Lu, J. Catal. 364 (2018) 271–281.
 - [18] W.F. Han, X.J. Li, H.D. Tang, Z.K. Wang, M. Xi, Y. Li, H.Z. Liu, J. Nanopart. Res. 17 (2015) 12.
 - [19] W.F. Han, B. Liu, X.L. Li, L.T. Yang, J.C. Wang, H.D. Tang, W.C. Liu, Ind. Eng. Chem. Res. 57 (2018) 12774–12783.
 - [20] W.F. Han, Z.K. Wang, X.J. Li, H.D. Tang, M. Xi, Y. Li, H.Z. Liu, J. Mater. Sci. 51 (2016) 11002–11013.
 - [21] H.L. Wang, W.F. Han, X.L. Li, B. Liu, H.D. Tang, Y. Li, Molecules 24 (2019) 12.
 - [22] W.Z. Jia, Q. Wu, X.W. Lang, C. Hu, G.Q. Zhao, J.H. Li, Z.R. Zhu, Catal. Lett. 145 (2015) 654–661.
 - [23] S. Celerier, F. Richard, Catal. Commun. 67 (2015) 26–30.
 - [24] Y.S. Chung, H. Lee, H.D. Jeong, Y.K. Kim, H.G. Lee, H.S. Kim, S. Kim, J. Catal. 175 (1998) 220–225.
 - [25] E. Kemnitz, Catal. Sci. Technol. 5 (2015) 786–806.
 - [26] W.F. Han, C.P. Zhang, H.L. Wang, S.L. Zhou, H.D. Tang, L.T. Yang, Z.K. Wang, Catal. Sci. Technol. 7 (2017) 6000–6012.
 - [27] S. Lim, M.S. Kim, J.W. Choi, H. Kim, B.S. Ahn, S.D. Lee, H. Lee, C.S. Kim, D.J. Suh, J.M. Ha, K.H. Song, Catal. Today 293 (2017) 42–48.
 - [28] F. Hiroyasu, K.E. Cordova, O.K. Michael, O.M. Yaghi, SCIENCE 341 (2013) 974.
 - [29] S. Kitagawa, R. Kitaura, S. Noro, Angew. Chemie Int. Ed. English 43 (2004) 2334–2375.
 - [30] S. Krause, V. Bon, I. Senkovska, U. Stoeck, D. Wallacher, D.M. Tobbens, S. Zander, R.S. Pillai, G. Maurin, F.X. Coudert, S. Kaskel, Nature 532 (2016) 348–352.
 - [31] B. Li, H.M. Wen, Y. Cui, W. Zhou, G. Qian, B.J.A.M. Chen, Adv. Mater. 28 (2016) 8819–8860.
 - [32] W.P. Lustig, S. Mukherjee, N.D. Rudd, A.V. Desai, J. Li, S.K. Ghosh, Chem. Soc. Rev. 46 (2017) 3242–3285.
 - [33] P.Z. Chen, T.P. Zhou, L.L. Xing, K. Xu, Y. Tong, H. Xie, L.D. Zhang, W.S. Yan, W.S. Chu, C.Z. Wu, Y. Xie, Angew. Chem. Int. Ed. Engl. 56 (2017) 610–614.
 - [34] M.F. Li, Z.P. Zhao, T. Cheng, A. Fortunelli, C.Y. Chen, R. Yu, Q.H. Zhang, L. Gu, B.V. Merinov, Z.Y. Lin, E.B. Zhu, T. Yu, Q.Y. Jia, J.H. Guo, L. Zhang, W.A. Goddard, Y. Huang, X.F. Duan, Science 354 (2016) 1414–1419.
 - [35] P. Liu, Y. Zhao, R. Qin, S. Mo, G. Chen, L. Gu, D.M. Chevrier, P. Zhang, Q. Guo, D. Zang, B. Wu, G. Fu, N. Zheng, Science 352 (2016) 797–801.
 - [36] X.F. Yang, A.Q. Wang, B.T. Qiao, J. Li, J.Y. Liu, T. Zhang, Acc. Chem. Res. 46 (2013) 1740–1748.
 - [37] Y. Chen, S. Ji, Y. Wang, J. Dong, W. Chen, Z. Li, R. Shen, L. Zheng, Z. Zhuang, D. Wang, Y. Li, Angew. Chem. Int. Ed. Engl. 56 (2017) 6937–6941.
 - [38] Q. Yang, C.-C. Yang, C.-H. Lin, H.-L. Jiang, Angew. Chem. Int. Ed. Engl. 58 (2019) 3511–3515.
 - [39] G. Ferey, C. Mellot-Draznieks, C. Serre, F. Millange, J. Dutour, S. Surble, I. Margiolaki, Science 309 (2005) 2040–2042.
 - [40] D.-Y. Hong, Y.K. Hwang, C. Serre, G. Ferey, J.-S. Chang, Adv. Funct. Mater. 19 (2009) 1537–1552.
 - [41] N. Tsumori, L. Chen, Q. Wang, Q.-L. Zhu, M. Kitta, Q. Xu, Chem 4 (2018) 845–856.
 - [42] X.-B. Meng, J.-L. Sheng, H.-L. Tang, X.-J. Sun, H. Dong, F.-M. Zhang, Appl. Catal. B 244 (2019) 340–346.
 - [43] X. Qiu, J. Chen, X. Zou, R. Fang, L. Chen, Z. Chen, K. Shen, Y. Li, Chem. Sci. 9 (2018) 8962–8968.
 - [44] R. Liu, J. Conradie, E. Erasmus, J. Electron. Spectrosc. Relat. Phenom. 206 (2016) 46–51.
 - [45] S. Gao, C. Dong, H. Luo, K. Xiao, X. Pan, X. Li, Electrochim. Acta 114 (2013) 233–241.
 - [46] X.-Z. Fu, X.-X. Luo, J.-L. Luo, K.T. Chuang, A.R. Sanger, A. Krzywicki, J. Power Sources 196 (2011) 1036–1041.
 - [47] J. Sloczynski, J. Janas, T. Machej, J. Rynkowski, J. Stoch, Appl. Catal., B 24 (2000) 45–60.
 - [48] Y. Lin, W. Cai, X. Tian, X. Liu, G. Wang, C. Liang, J. Mater. Chem. 21 (2011) 991–997.
 - [49] W.-X. Zhang, Y. Liang, J.-W. Luo, A.-P. Jia, Y.-J. Wang, J.-Q. Lu, M.-F. Luo, J. Mater. Sci. 51 (2016) 6488–6496.
 - [50] W. Mao, Y. Bai, B. Wang, W. Wang, H. Ma, Y. Qin, C. Li, J. Lu, Z.W. Liu, Appl. Catal. B 206 (2017) 65–73.
 - [51] C.H. Bartholomew, Appl. Catal. A Gen. 212 (2001) 17–60.
 - [52] X.X. Fang, Y. Wang, W.Z. Jia, J.D. Song, Y.J. Wang, M.F. Luo, J.Q. Lu, Appl. Catal. A Gen. 576 (2019) 39–46.
 - [53] J. Li, G. Xiong, Z. Feng, Z. Liu, Q. Xin, C.J.M. Li, M. Materials 39 (2000) 275–280.